Surface Adsorption-Mediated Ultrahigh Efficient Peptide Encapsulation with a Precise Ratiometric Control for Type 1 and 2 Diabetic Therapy

Zhang, Pei

2022-04

NANO · MICRO
small
www.small-journal.com

Surface Adsorption-Mediated Ultrahigh Efficient Peptide Encapsulation with a Precise Ratiometric Control for Type 1 and 2 Diabetic Therapy

Pei Zhang, Chunyang Du, Tianhe Huang, Shuai Hu, Yuancheng Bai, Cong Li, Guobing Feng, Yue Gao, Zhi Li, Baoxun Wang, Jouni T. Hirvonen, Jin Fan, Hélder A. Santos,* and Dongfei Liu*

A surface adsorption strategy is developed to enable the engineering of microcomposites featured with ultrahigh loading capacity and precise ratiometric control of co-encapsulated peptides. In this strategy, peptide molecules (insulin, exenatide, and bivalirudin) are formulated into nanoparticles and their surface is decorated with carrier polymers. This polymer layer blocks the phase transfer of peptide nanoparticles from oil to water and, consequently, realizes ultrahigh peptide loading degree (up to 78.9%). After surface decoration, all three nanoparticles are expected to exhibit the properties of adsorbed polymer materials, which enables the co-encapsulation of insulin, exenatide, and bivalirudin with a precise ratiometric control. After solidification of this adsorbed polymer layer, the release of peptides is synchronously prolonged. With the help of encapsulation, insulin achieves 8 days of glycemic control in type 1 diabetic rats with one single injection. The co-delivery of insulin and exenatide (1:1) efficiently controls the glycemic level in type 2 diabetic rats for 8 days. Weekly administration of insulin and exenatide co-encapsulated microcomposite effectively reduces the weight gain and glycosylated hemoglobin level in type 2 diabetic rats. The surface adsorption strategy sets a new paradigm to improve the pharmacokinetic and pharmacological performance of peptides, especially for the combination of peptides.

1. Introduction

Since the discovery of insulin in 1922, peptides play an increasingly important role in the treatment of various disease, such as diabetes, cancer, infectious diseases, and autoimmune diseases.[1–6] Because of their poor permeability and easy inactivation in gastrointestinal tract, most peptide therapeutics are administrated through injections in solution form.[7,8] Nevertheless, peptides need frequent and repeated administration due to their short plasma half-life, which leads to peak-and-valley pharmacokinetics, poor tolerability, and safety concerns. Encapsulation is an effective strategy to improve the pharmacokinetic and pharmacodynamic properties of peptide therapeutics.[9–11] For widely used polymeric and lipophilic materials, their poor miscibility with peptide molecules inherently limited peptide loading capacity in the matrix.[12–14] As a result, most peptide-encapsulated systems are

P. Zhang, C. Du, T. Huang, S. Hu, Y. Bai, G. Feng, Y. Gao, Z. Li, B. Wang, D. Liu
State Key Laboratory of Natural Medicines
Department of Pharmaceutical Science
China Pharmaceutical University
Nanjing 210009, China
E-mail: dongfei.liu@cpu.edu.cn
P. Zhang, J. T. Hirvonen, H. A. Santos, D. Liu
Drug Research Program
Division of Pharmaceutical Chemistry and Technology
Faculty of Pharmacy
University of Helsinki
Helsinki 00014, Finland
E-mail: h.a.santos@umcg.nl

C. Du, T. Huang, S. Hu, Y. Bai, G. Feng, Y. Gao, Z. Li, B. Wang, D. Liu
NMPA Key Laboratory for Research and Evaluation of Pharmaceutical Preparations and Excipients
China Pharmaceutical University
Nanjing 210009, China
C. Li, J. Fan
Department of Orthopaedics
The First Affiliated Hospital of Nanjing Medical University
Nanjing 210029, China
H. A. Santos
Department of Biomedical Engineering
W.J. Kolff Institute for Biomedical Engineering and Materials Science
University Medical Center Groningen/University of Groningen
Ant. Deusinglaan 1, Groningen 9713 AV, The Netherlands

ADVANCED
SCIENCE NEWS
www.advancedsciencenews.com

NANO · MICRO
small
www.small-journal.com

composed primarily of nontherapeutic hosting materials. The poor loading capacity constrains the enhancement of treatment efficacy by encapsulation, intensifies carrier materials-related side effects, and restricts the patient compliance improvement,[15,16] which hinders the clinical application of peptide-encapsulated systems.

Combination therapy is widely adopted in clinical practice to enhance the therapeutic efficacy of each drug for various disease treatments.[17–22] For type 2 diabetic patients, combination therapy must be considered when the level of glycosylated hemoglobin (HbA1c) is equal to or greater than 9.0%.[23] The combination of basal insulin and a glucagon-like peptide 1 (GLP-1) receptor agonist can improve glycemic control, lower hypoglycemic risk, and alleviate body weight gain of type 2 diabetic patients.[24] In comparison with monotherapy, combination of buserelin and tamoxifen was more effective in the treatment of advanced breast cancer for premenopausal patients.[25] The overall survival of patients co-administrated with buserelin and tamoxifen (3.7 years) was much longer than that of patients treated with buserelin (2.5 years) or tamoxifen (2.9 years) alone.[25] Due to their diverse structures, peptide molecules show different affinity to carrier materials and, consequently, result in the poor ratiometric control of encapsulated peptide molecules. Therefore, the simultaneous incorporation of multiple therapeutics into a single carrier is still a remarkable challenge.[26,27]

Herein, we proposed a surface adsorption strategy to enable high loading capacity, ratiometric control, and synchronous release of peptide therapeutics (**Figure 1**a). In this strategy, peptide therapeutics were formulated into nanoparticles and their surface was decorated with carrier materials. The adsorbed material layer is supposed to stabilize peptide nanoparticles in oil phase and inhibit their phase transfer into water phase. Compared with physicochemical features of therapeutics molecules, the surface properties of therapeutics nanoparticles, such as hydrophobicity and surface charge, are relatively limited. After surface adsorption, peptide nanoparticles are supposed to uniformly exhibit the properties of adsorbed materials. This uniform surface property may enable the co-encapsulation of multiple types of peptides with a precise ratiometric control. Moreover, the solidification of this adsorbed material layer may synchronously prolong the release of co-encapsulated multiple types of peptides.

In this study, insulin and exenatide were selected as the model therapeutics, whose pharmacokinetics properties are urgent to be improved in clinics.[28–31] Another peptide, bivalirudin, was incorporated to illustrate the versatility of surface adsorption strategy in ratiometric control over therapeutics encapsulation. Since long-acting injectable microspheres based on biodegradable poly(lactide-co-glycolide) (PLGA) have been widely used in clinic, this polymer terminated with ester group was selected as the control carrier material (Figure S1, Supporting Information). As electrostatic attraction usually plays a dominant role in surface adsorption,[32–34] a cationic spermine was conjugated to PLGA (PLGS) to facilitate the surface decoration. Benefiting from the adsorption of PLGS, the obtained microcomposites merged ultrahigh mass fraction of peptides (up to 78.9%) and ratiometric control and synchronous release of co-encapsulated peptide therapeutics. The fabricated insulin-encapsulated microcomposites (INS@PLGS) achieved 8 days of glycemic control in type 1 diabetic rats. Microcomposites co-incorporated with insulin and exenatide (INS+EXT@PLGS) efficiently controlled the glycemic level in type 2 diabetic rats for 8 days.

2. Results and Discussion

2.1. Surface Adsorption Blocks Phase Transfer of Peptide Nanoparticles

To evaluate the feasibility of surface adsorption strategy, we studied the adsorption of polymer molecules onto insulin and exenatide particles using a quartz crystal microbalance. This microbalance is an ultrasensitive mass balance that measures nanogram to microgram level mass changes by monitoring the oscillation frequency of a quartz crystal.[35,36] After spin-coating peptide particles, a layer of insulin or exenatide film formed on the quartz disc. For this quartz disc, the decrease of the third overtone oscillation frequency (ΔF_3) reflected the adsorption of polymer molecules, when polymer solution (10 mg mL^{-1} in dimethyl carbonate) flowed over its surface (Figure 1b). After rinsing with dimethyl carbonate, the ΔF_3 caused by the adsorption of PLGA and solvent molecules was -8.5 ± 1.1 Hz for insulin film and -12.9 ± 2.1 Hz for exenatide film (see Figure S2, Supporting Information). The ΔF_3 caused by the adsorption of PLGS together with solvent molecules (-23.5 ± 3.9 Hz for insulin, -84.3 ± 7.6 Hz for exenatide) was significantly ($P < 0.01$ for insulin, $P < 0.001$ for exenatide) higher than that of PLGA. Quartz crystal microbalance results indicated that more PLGS molecules were absorbed onto the surface of insulin and exenatide nanoparticles, when compared with PLGA. The isoelectric point of insulin and exenatide is around 5.3[37] and 4.9,[38] respectively. Both peptides have abundant acid residues in their structures. The resulting strong electrostatic attractions between cationic PLGS and insulin or exenatide might be the reason why more PLGS molecules were adsorbed onto the surface of insulin or exenatide nanoparticles.

Then, we studied the effect of absorbed polymers on the particle size and polydispersity index of insulin and exenatide particles. Insulin and exenatide nanoparticles were not stable and aggregated into microscale in dimethyl carbonate (Figure 1c). In comparison with bare peptide particles, the addition of PLGS significantly decreased the size of insulin (approximately 272 nm; $P < 0.001$) and exenatide particles (approximately 415 nm; $P < 0.01$) in dimethyl carbonate. The corresponding polydispersity index of insulin particles decreased remarkably ($P < 0.05$) from 0.27 to 0.12, and that of exenatide particles decreased significantly ($P < 0.001$) from 0.42 to 0.12. After the addition of PLGA, such size decrease and dispersity improvement effects were not observed for insulin particles. The size and polydispersity index of exenatide particles decreased with the help of PLGA, but the size of exenatide particles was still in microscale. It seemed that the surface adsorption of PLGS improved the stability of insulin and exenatide nanoparticles in dimethyl carbonate. The adsorbed cationic PLGS molecules offer strong steric hindrance and electrostatic repulsion among the polymer-adsorbed peptide nanoparticles, which can efficiently stabilize peptide nanoparticles and can avoid their aggregation.[39,40]
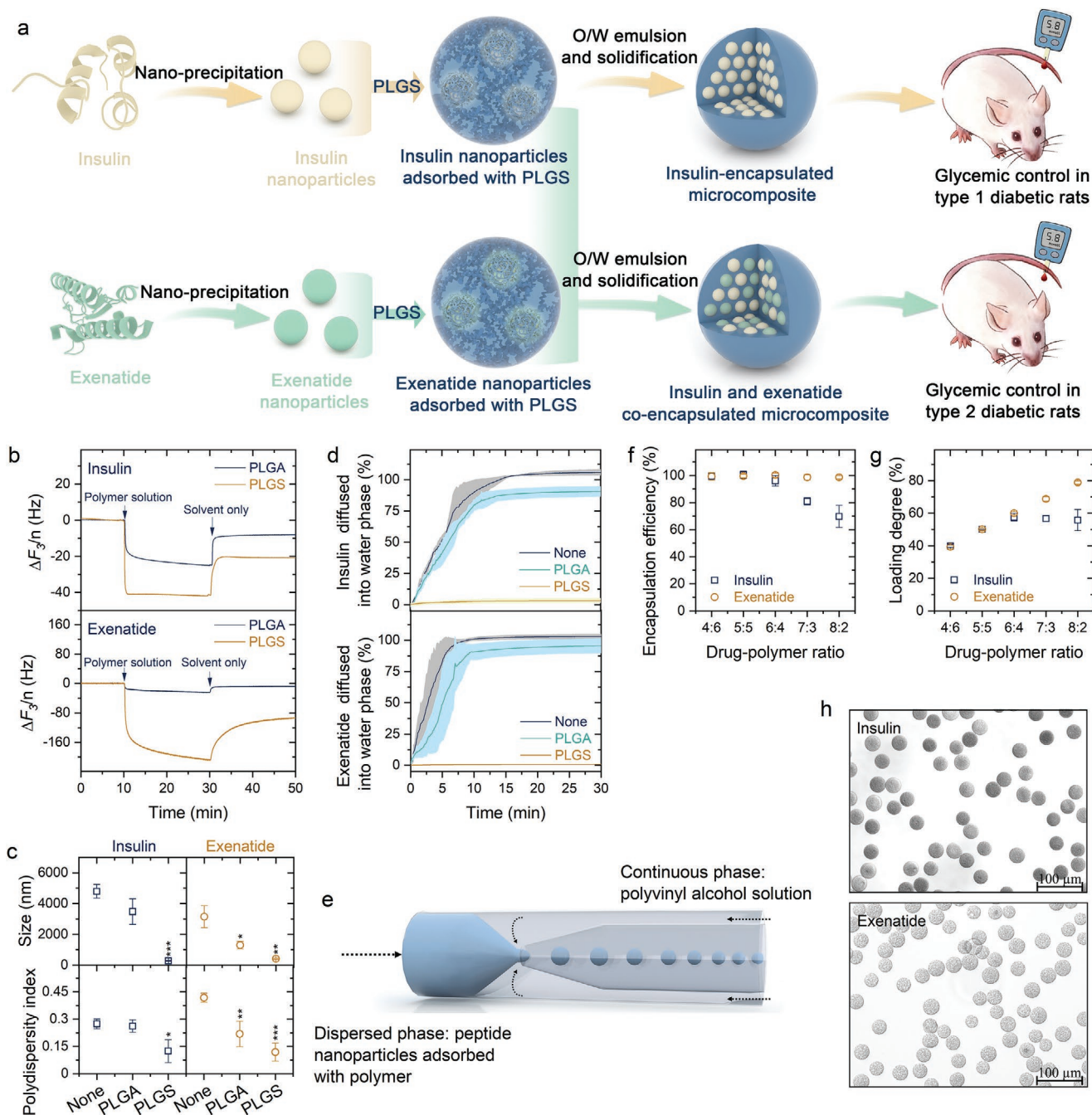
ADVANCED
SCIENCE NEWS
www.advancedsciencenews.com

NANO · MICRO
small
www.small-journal.com

Figure 1. Surface adsorption blocks phase transfer of peptide nanoparticles. a) Schematic illustration of surface adsorption strategy and its application in diabetic therapy. b) The frequency change of third overtone (ΔF_3) as a function of time when PLGA or PLGS flowed over the quartz disc coated with insulin or exenatide particles. c) The size and polydispersity index of insulin and exenatide particles before and after surface adsorption with polymers (PLGA or PLGS, $n = 3$). d) The effect of PLGA and PLGS on the phase transfer of peptide (insulin and exenatide) particles from dimethyl carbonate to water ($n = 3$). The initial concentration of peptides and polymers (PLGA or PLGS) in dimethyl carbonate was 10 mg mL^{-1}. e) Schematic illustration of the microfluidic device for microcomposite engineering. f,g) The encapsulation efficiency (f) and drug loading degree (g) of insulin and exenatide in PLGS microcomposites with various drug-polymer ratios ($n = 3$). h) The light microscope picture of INS@PLGS and EXE@PLGS microcomposites with drug-polymer ratio of 5:5. The term None refers to the group without polymers. Both PLGA and PLGS groups were compared with the None group; the level of significance was set at a probability of * $P < 0.05$, ** $P < 0.01$ and ***$P < 0.001$.

We argue that the adsorbed polymer layer is feasible to hinder the phase transfer of insulin and exenatide particles into water phase as long as the surface adsorption is compact enough. To verify this hypothesis, we stacked 1.5 mL of water on the top of 0.5 mL dimethyl carbonate-containing insulin or exenatide particles (10 mg mL^{-1}) and measured the percentage of peptide transferred into water phase. For the group without any polymer molecules, nearly 100% of insulin and exenatide transferred into

the water phase in 30 min (Figure 1d). With the help of PLGS, the transfer fraction of peptide decreased to $3.19 \pm 1.62\%$ and $0.75 \pm 0.04\%$ for insulin and exenatide, respectively. As expected, the adsorbed PLGS layer successfully hindered the phase transfer of insulin and exenatide nanoparticles into water. PLGA only slightly slowed the phase transfer of insulin ($90.6 \pm 4.1\%$) and exenatide ($95.6 \pm 5.7\%$) in 30 min. This limited phase transfer blocking capability of PLGA (10 mg mL^{-1}) could be ascribed to the partial surface coverage for peptide particles with PLGA molecules.

Insulin or exenatide-encapsulated PLGS microcomposites, INS@PLGS and EXE@PLGS, were fabricated using a flow-focusing device (Figure S3, Supporting Information, and Figure 1e). PLGS dimethyl carbonate solution containing insulin or exenatide nanoparticles served as the dispersed phase, while continuous phase is polyvinyl alcohol solution (1%, w/v). Polyvinyl alcohol served as the emulsifier to stabilize the formed oil-in-water droplets. The dispersed and continuous phases were pumped into outer capillary and the space between outer and inner capillaries, respectively, in opposite direction. The oil-in-water emulsions formed in the inner capillary solidified into microcomposites as the dimethyl carbonate depleted into polyvinyl alcohol solution.

For all drug-polymer weight ratios studied, the encapsulation efficiency (percentage of the encapsulated drug among the initially added drug) of exenatide in microcomposites was higher than 98% (Figure 1f). When the drug-polymer ratio increased from 4:6 to 8:2, the corresponding loading degree (weight ratio of drug in the microcomposites) climbed from 39.3% to 78.9%, which is ultrahigh for peptide therapeutics (Figure 1g). However, by increasing the insulin-PLGS weight ratio from 6:4 to 8:2, the insulin loading degree in microcomposites was kept at approximately 55%. When PLGS served as carrier materials, the encapsulation efficiency of exenatide was higher than that of insulin. This was consistent with the results of quartz crystal microbalance, for which the adsorbed mass of PLGS and solvents onto exenatide nanoparticles surface were higher than that of insulin. Furthermore, all obtained INS@PLGS and EXE@PLGS with different drug-polymer ratios were spherical with narrow size distributions (Figure 1h and Figures S4 and S5, Supporting Information). Their polydispersity indexes (the ratio between the standard deviation and the mean diameter of particles multiplied by 100%) fluctuated within a range between 4.2% and 8.3%. Besides, the encapsulated insulin and exenatide were in an amorphous state (Figure S6, Supporting Information).

Collectively, compared with PLGA, more PLGS molecules adsorbed onto the surface of insulin or exenatide particles. This layer of carrier polymer could stabilize the insulin or exenatide nanoparticles in dimethyl carbonate and efficiently inhibit their phase transfer into water phase. The fabricated microcomposites realized ultrahigh encapsulation efficiency for insulin and exenatide, and consequently, achieved ultrahigh peptide loading degree up to 78.9%.

2.2. Surface Adsorption Enables a Precise Ratiometric Control Over the Loading of Multiple Types of Peptides

After surface adsorption, peptide nanoparticles are supposed to uniformly exhibit the properties of adsorbed materials.

Therefore, we argued that this surface adsorption strategy can also achieve simultaneous encapsulation of multiple types of peptides into a single microcomposite with a precise ratiometric control. Surface adsorption strategy enables efficient encapsulation of insulin and exenatide separately. With the help of ultrahigh encapsulation efficiency of each peptide, we could transform the ratiometric control over the co-encapsulated multiple peptides to their initial weight ratio in the formulation.

The overall peptide-polymer ratio was fixed at 5:5 to ensure the ultrahigh encapsulation efficiency for each peptide. To verify the capability of surface adsorption strategy in co-encapsulation of multiple peptides, microcomposites with a variety of insulin-exenatide weight ratios (1:9, 5:5, and 9:1) were engineered. As expected, insulin and exenatide were efficiently co-encapsulated into the microcomposites, regardless of insulin-exenatide weight ratios (**Figure 2**a). The loading degree of insulin was plotted against the corresponding loading degree of exenatide. A good linear correlation ($R^2 = 0.9989$) between the loading degree of insulin and exenatide was observed (Figure 2b). The slope of the linear fitting was 0.9995, suggesting that the loading degree of insulin and exenatide in the micocomposites could be precisely controlled by simply adjusting the initial insulin-exenatide weight ratio. Deducing from the intercept of the linear fitting, total mass fraction of insulin and exenatide in the microcomposites was 49.7%, which was quite close to the feed peptide-polymer ratio (5:5).

To verify the versatility of our surface adsorption strategy in precise ratiometric control over the co-encapsulation of multiple peptides, the third peptide (bivalirudin) was incorporated into PLGS microcomposites. For the encapsulation of only bivalirudin, its encapsulation efficiency fluctuated within a range between 95.0% and 99.4% when the weight ratio between bivalirudin and PLGS increased from 4:6 to 8:2 (see Figure S7, Supporting Information). The loading degree of bivalirudin in the obtained microcomposite was up to 76.1%. Bivalirudin was co-encapsulated with insulin and exenatide, respectively, with different peptide ratios (1:9, 5:5, and 9:1). Microcomposite co-encapsulated with insulin and bivalirudin revealed ultrahigh encapsulation efficiency (> 97%) for each peptide; the loading degree ratios between insulin and bivalirudin were always in accordance with their initial weight ratios (Figure 2c,d). Similar results were observed for the microcomposite co-encapsulated with bivalirudin and exenatide (Figure 2e,f).

We further simultaneously encapsulated three peptides, insulin, exenatide, and bivalirudin, into a single microcomposite with a weight ratio of 1:1:1. Almost all insulin (98.2%), exenatide (95.8%), and bivalirudin (97.9%) was encapsulated and the ratio of their mass inside the microcomposite was close to 1:1:1 (Figure 2g,h). All the obtained dual- or triple- drug encapsulated microcomposites were spherical with narrow size distributions (Figure 2i and Figures S8 and S9, Supporting Information). Furthermore, the measured residual polyvinyl alcohol in the fabricated INS+EXE@PLGS microcomposites was $0.93 \pm 0.15\%$ (Figure S10, Supporting Information).

Surface adsorption strategy enables efficient encapsulation of peptides. With the help of ultrahigh encapsulation efficiency of each peptide, we could precisely control the loading degree ratio for each peptide by simply adjusting their initial weigh ratio in the formulation. Our surface adsorption strategy
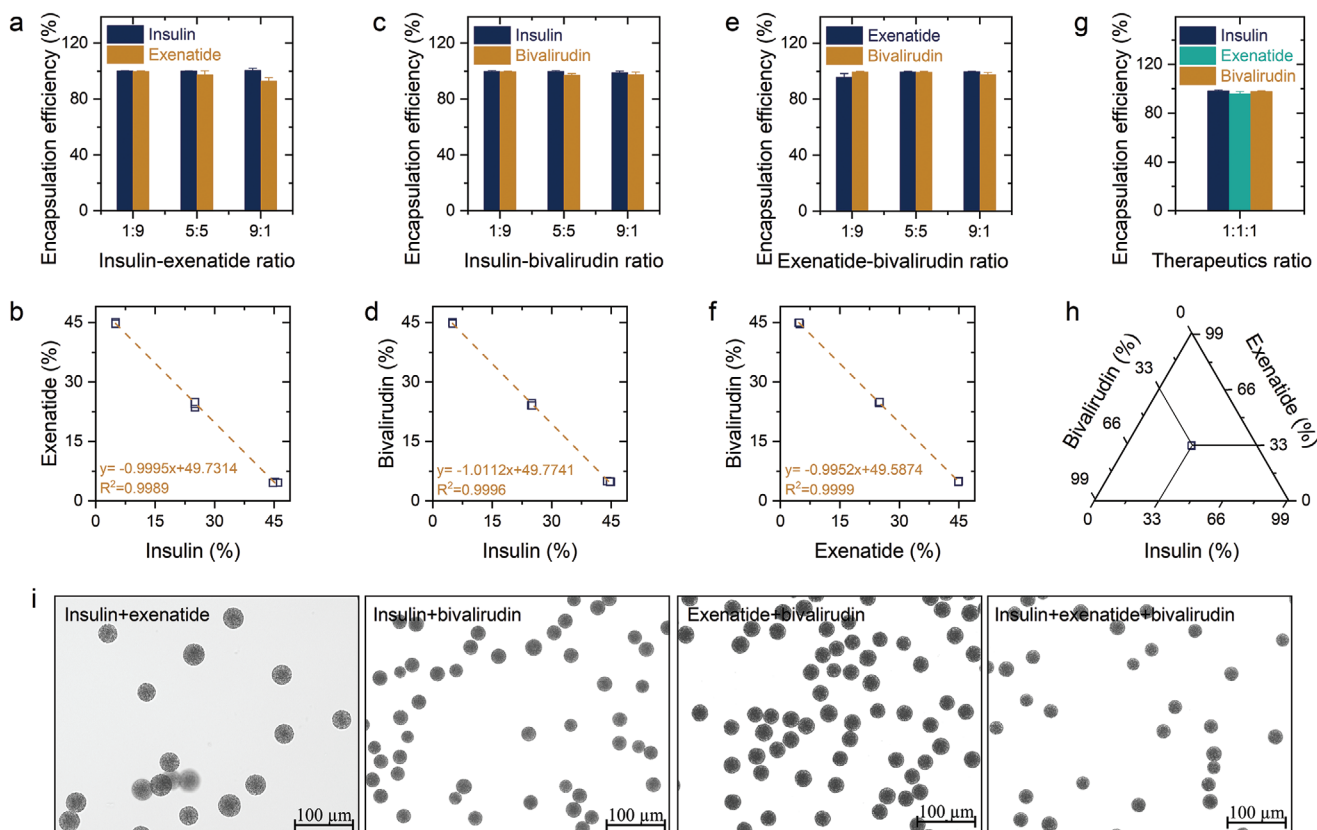
ADVANCED
SCIENCE NEWS
www.advancedsciencenews.com

NANO · MICRO
small
www.small-journal.com

Figure 2. Surface adsorption enables a precise ratiometric control over the loading of multiple types of peptides. For all the tests, the overall drug-polymer ratio was fixed at 5:5. a,b) The effect of feeding weight ratio between insulin and exenatide on the encapsulation efficiency (a) and loading degree (b) of each peptide ($n = 3$). c,d) The effect of feeding weight ratio between insulin and bivalirudin on the encapsulation efficiency (c) and loading degree (d) of each peptide ($n = 3$). e,f) The effect of feeding weight ratio between exenatide and bivalirudin on the encapsulation efficiency (e) and loading degree (f) of each peptide ($n = 3$). g,h) The effect of feeding weight ratio between insulin, exenatide, and bivalirudin (1:1:1) on the encapsulation efficiency (g) of each peptide and the overall weight ratio among three peptides (h) in the obtained microcomposite ($n = 3$). i) The light microscope picture of dual-peptides loaded microcomposites with peptide ratio of 5:5 and triple-peptides loaded microcomposites with peptide ratio of 1:1:1.

provided a solution to the long-standing challenge in precise ratiometric control over the encapsulation of therapeutics into a single drug delivery carrier. This strategy is potential to be applied in the encapsulation of more types of peptides with a precise ratiometric control.

2.3. Insulin-Encapsulated Microcomposite Persists Blood Glycemic Control on Type 1 Diabetes for 8 Days

Insulin is an important therapeutic agent for diabetes treatment, especially for the type 1 diabetes.[41–45] Nevertheless, patients need several insulin injections per day to persist their blood glucose concentration within the normal range. Therefore, a system with a long-term sustained insulin release profile and an ultrahigh mass fraction of insulin would be highly desirable for diabetes therapy. To verify the pharmacological performance of the system engineered by our surface adsorption strategy, we evaluated the therapeutic efficiency of INS@PLGS in rats with type 1 diabetes.

At first, we studied the impact of insulin-PLGS weight ratio on the insulin release profile. The engineered microcomposites enabled the sustained release of insulin for up to 45 days,

depending on the insulin-PLGS ratio. By reducing the insulin-PLGS ratio from 7:3 to 4:6, the insulin released was decreased from approximately 21.8% to approximately 8.3% on the first day. After extending the release period to 20 days, the fraction of insulin released from INS@PLGS was approximately 22.8% at the insulin-polymer ratio of 4:6; this released fraction increased to approximately 63.3% when the insulin-PLGS ratio was 7:3 (**Figure 3**a). It seemed that the insulin release rate could be controlled by adjusting the polymer weight ratio. High drug loading degree could adversely affect the release profiles of microcomposites. However, all types of obtained microcomposites successfully realized gradual insulin release. This good control of insulin release could be ascribed to the adsorbed PLGS molecules on the surface of each insulin nanoparticle. After the solidification of droplets, these adsorbed PLGS molecules could form a polymer layer on each nanoparticle, which was supposed to sustain the release of insulin.

The peptide structure and its biological activity are strongly correlated; thus, we verified the structure of released insulin molecules. As shown in Figure 3b, no obvious difference was observed between the circular dichroism spectrum of released and native insulin molecules. The molar ellipticity ratio between the band at 208 and 223 nm ($[\Phi]208/[\Phi]223$) could

ADVANCED
SCIENCE NEWS
www.advancedsciencenews.com

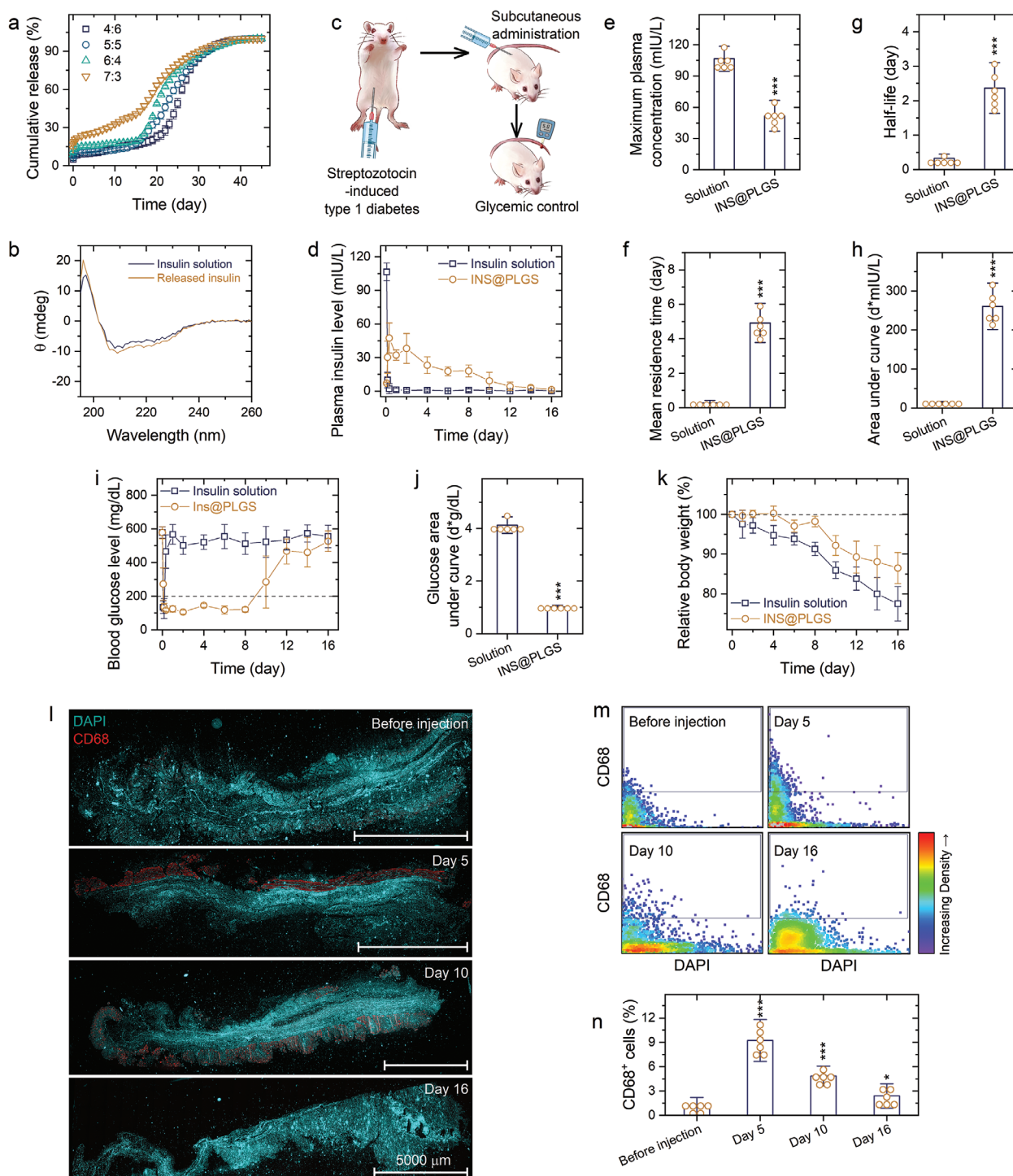NANO · MICRO
small
www.small-journal.com

Figure 3. Insulin-encapsulated microcomposite persists blood glycemic control on type 1 diabetes for 8 days. a) Effect of insulin-PLGS weight ratios on the release profile of INS@PLGS ($n = 3$). b) Circular dichroism spectra of native and released insulin. c) Schematic diagram of in vivo study in type 1 diabetic rats. d) Plasma insulin level of type 1 diabetic rats administrated with insulin solution and INS@PLGS ($n = 6$). e–h) The maximum plasma concentration (e), mean residence time (f), half-life (g), and area under curve (h) of insulin solution and INS@PLGS deduced from the plasma concentration-time curve ($n = 6$). i) Blood glucose levels of type 1 diabetic rats administrated with insulin solution and INS@PLGS ($n = 6$). j) The glucose area under curve calculated from the curve of blood glucose level versus time over 8 days after administration ($n = 6$). The level of significance was set at the probability of ***$P < 0.001$. k) Body weight of type 1 diabetic rats administrated with insulin solution and INS@PLGS ($n = 6$). l) Immuno-fluorescent staining of cell nuclei (DAPI, in cyan) and CD68 (in red) of tissues adjacent to the injection site before injection and at 5, 10, and 16 days after administration. m,n) Representative VTEA scatterplots of immunofluorescent stained cells (m) and the relative quantitation of CD68-positive cells around the injection site (n, $n = 6$). The data of days 5, 10, and 16 after administration were compared with that of before injection. The level of significance was set at probabilities of *$P < 0.05$ and ***$P < 0.001$.

**ADVANCED
SCIENCE NEWS**
www.advancedsciencenews.com

**NANO · MICRO
small**
www.small-journal.com

qualitatively indicate the overall conformation of insulin molecules.[46,47] This [Φ]208/[Φ]223 value for released insulin molecules (1.39) was close to that of native ones (1.29), suggesting that microcomposite engineering and drug release process had no obvious effect on the conformation of insulin molecules. Even at a concentration of 10 mg mL^{-1}, PLGS microparticles showed no significant impact on the viability of primary dermal fibroblast cells and RAW 246.7 macrophages (Figure S11, Supporting Information), indicating the great potential of PLGS as carrier materials in drug delivery.

We employed streptozotocin-induced type 1 diabetic rats as the animal model to evaluate the glycemic control ability of INS@PLGS prepared by the surface adsorption strategy. As illustrated in Figure 3c, Sprague–Dawley (SD) rats were injected intraperitoneally with a dose of 50 mg kg^{-1} streptozotocin to destruct pancreas islet B cells and induce type 1 hyperglycemia. The type 1 diabetic rats were divided into four groups, which were subcutaneously injected with insulin solution (10 IU kg^{-1}), INS@PLGS (drug-polymer ratio of 5:5, 100 IU kg^{-1}), normal saline (N.S.), and bare PLGS microparticles. Normal rats served as a control.

For insulin solution, the plasma insulin concentration increased dramatically and peaked at 106.5 ± 8.0 mIU L^{-1} after 2 h (Figure 3d,e). This plasma insulin concentration declined to lower than 2 mIU L^{-1} after 1 day. In contrast, INS@PLGS with an insulin loading degree of 49.3% maintained the plasma insulin level higher than 17 mIU L^{-1} for at least 8 days and reached a peak of 47.4 ± 13.4 mIU L^{-1} at 8 h after administration. After encapsulation into microcomposites, the mean residence time was 17.0 times longer than that of insulin solution (Figure 3f); the half-life of insulin was significantly ($P < 0.001$) prolonged from 0.3 days to 2.4 days (Figure 3g). The area under the plasma concentration-time curve of insulin solution and INS@PLGS were 12.2 ± 2.7 and 260.8 ± 39.8 mIU L^{-1} day, respectively (Figure 3h). After adjusting the dose of insulin administrated, the relative bioavailability of INS@PLGS was 2.1 times of insulin solution.

For INS@PLGS group, the blood glucose level of type 1 diabetic rats reduced gradually to normoglycemic range (< 200 mg dL^{-1}) at 4 h after administration and maintained lower than 200 mg dL^{-1} for at least 8 days (Figure 3i). After 12 days, the rats administrated with INS@PLGS returned to the initial hyperglycemic state (> 200 mg dL^{-1}). In contrast, insulin solution reduced the glycemia rapidly to 133.2 ± 36.6 mg dL^{-1} within 2 h and returned back to hyperglycemic state (464.7 ± 98.8 mg dL^{-1}) after 8 h. Consequently, the glucose area under the curve of INS@PLGS group was obviously ($P < 0.001$) lower than that of insulin solution group (Figure 3j). These results were in conformity with the pharmacokinetic results of insulin solution and INS@PLGS. As expected, normal saline and bare PLGS had no significant effect on the glycemic level of type 1 diabetic rats (see Figure S12, Supporting Information).

Bodyweight loss is one of the main clinical symptoms of type 1 diabetes. For INS@PLGS group, rats revealed relatively stable body weight levels within 8 days (Figure 3k). From day 10 after administration, rats in INS@PLGS group started to lose weight, which can be ascribed to the exhaustion of insulin. Rats treated with insulin solution, normal saline, or bare microparticles showed similar body weight profiles, which declined steadily during the whole therapy period (see Figure S13, Supporting Information). On the contrary, rats in non-diabetic control group gained weight gradually. These results implied that INS@PLGS was able to protect the rats from losing bodyweight.

We assessed the inflammatory response of host tissue administrated with INS@PLGS by monitoring the local level of macrophages. Therefore, tissues were stained with 6-Diamino-2-phenylindoadihydrochloride (DAPI; in cyan) and CD68 (in red) to identify the host cells and macrophages accumulated around the injection site (Figure 3l). The fraction of CD68-positive cells near the administrated microcomposites was qualified through volumetric tissue exploration and analysis[48] (VTEA, Figure 3m,n). Compared with the normal tissues ($1.2 \pm 0.7\%$), the CD68 positive cells increased significantly ($P < 0.001$) to $9.2 \pm 1.7\%$ in the tissues adjacent to the injection site at day 5 after administration. At day 10 after administration, macrophage cells accumulated in the injection site decreased to $4.9 \pm 0.8\%$. Most importantly, there was little evidence of macrophage cells recruitment ($2.4 \pm 1.0\%$) after 16 days. These histochemistry results indicated that the administration of exogenous microcomposites led to an acute short-term inflammatory response.

The pharmacokinetic study showed that INS@PLGS successfully prolonged the mean residence time and half-life of insulin, and efficiently enhanced insulin bioavailability. Despite its high insulin loading degree (approximately 49.3%), INS@PLGS realized an 8-day tight glycemic control within normal range and alleviated bodyweight loss in type 1 diabetic rats. As a result, the INS@PLGS efficiently reduced the insulin administration frequency, improved the patient compliance, and enhanced the therapeutic outcome of insulin.

2.4. Co-Delivery of Insulin and Exenatide Efficiently Controls the Glycemic Level in Type 2 Diabetic Rats for 8 Days

The combination of basal insulin plus a GLP-1 receptor agonist is an optional treatment strategy for type 2 diabetes.[24,49] Two fixed-ratio coformulations of insulin and GLP-1 receptor agonist, iGlarLixi and iDegLira, have been approved for type 2 diabetes therapy in clinic.[24,49] However, both coformulations are required to be administrated once daily, which can scarify the compliance of patients. Since INS@PLGS successfully improved the pharmacokinetic feature of insulin, we hypothesized that the microcomposite co-encapsulated with insulin and exenatide (a GLP-1 receptor agonist) was capable to optimize the pharmacokinetic features of insulin and exenatide synchronously.

One of the fixed-ratio coformulations, iDegLira, is a combination pen device that simultaneously delivers iDeg (a basal insulin, 100 units mL^{-1}) and liraglutide (a GLP-1 receptor agonist, 3.6 mg mL^{-1}).[24] To achieve equal treatment efficiency towards iDegLira, we employed the same ratio of basal insulin and GLP-1 receptor agonist inside the microcomposite. Taking molecular weight into consideration, the weight ratio of insulin and exenatide should be 1.04:1 for the dual-peptide encapsulated microcompoiste, INS+EXE@PLGS. Therefore, we engineered INS+EXE@PLGS with insulin-exenatide-PLGS weight ratio of 2.5:2.5:5 and evaluated its therapeutic efficiency for type 2 diabetes.
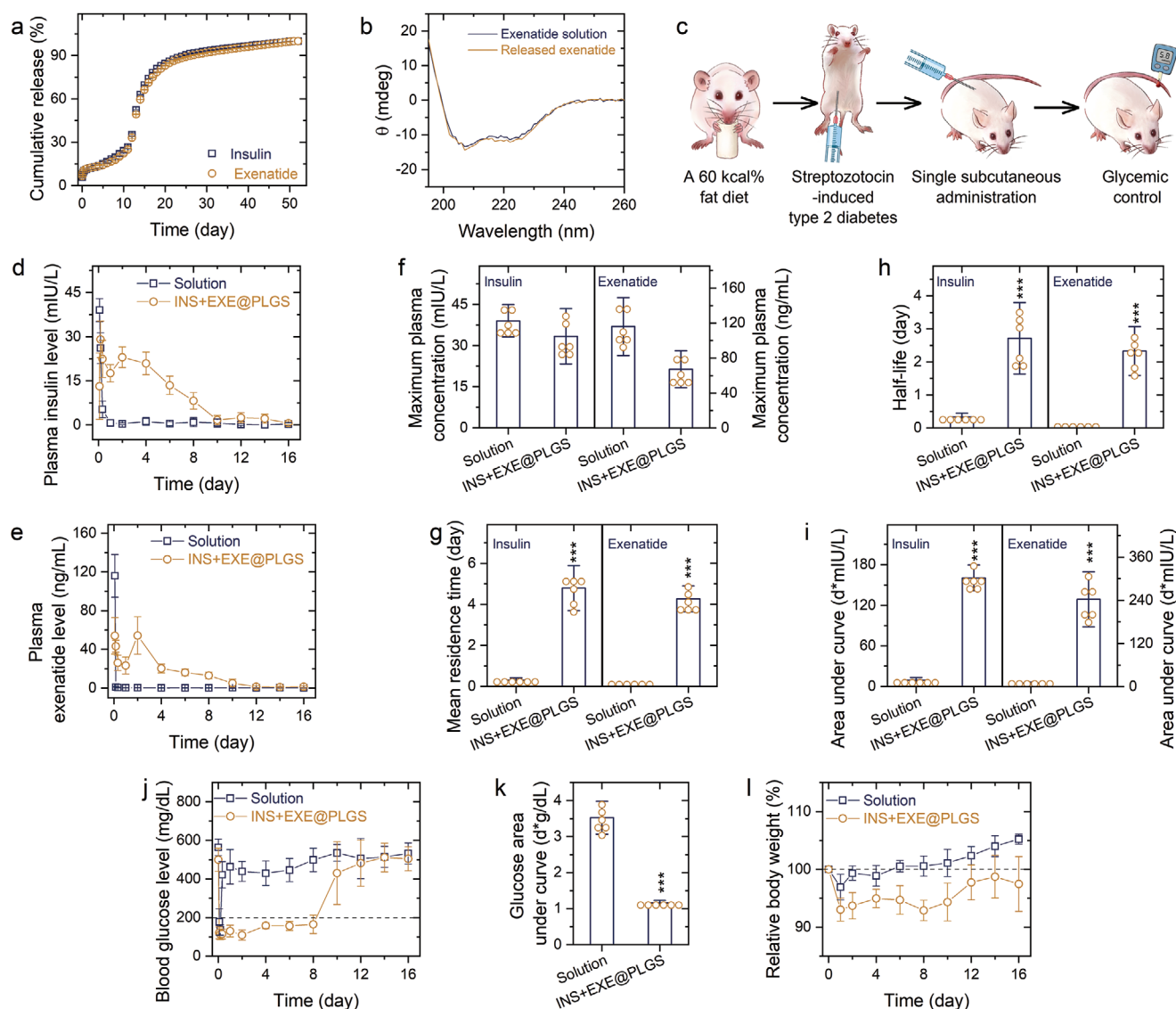
Figure 4. Co-delivery of insulin and exenatide efficiently controls the glycemic level in type 2 diabetic rats for 8 days. a) Release profiles of insulin and exenatide from INS+EXE@PLGS ($n = 3$). b) Circular dichroism spectra of native and released exenatide. c) Schematic diagram of in vivo study in type 2 diabetic rats. d,e) Plasma insulin (d) and exenatide (e) level of type 2 diabetic rats administrated with insulin&exenatide solution and INS+EXE@PLGS ($n = 6$). f–i) The maximum plasma concentration (f), mean residence time (g), half-life (h), and area under curve (i) of insulin&exenatide solution and INS+EXE@PLGS deduced from their plasma concentration-time curve ($n = 6$). j) Blood glucose levels of rats administrated with insulin&exenatide solution and INS+EXE@PLGS ($n = 6$). k) The glucose area under curve calculated from the curve of blood glucose level versus time over 8 days after administration ($n = 6$). l) Body weight of rats administrated with insulin&exenatide solution and INS+EXE@PLGS ($n = 6$). The level of significance was set at a probability of ***$P < 0.001$.

Synchronous release is the prerequisite for INS+EXE@PLGS to realize a fixed-ratio combination therapy for type 2 diabetes. As shown in **Figure 4**a, the insulin release profile excellently coincided with that of exenatide, which might be because the adsorbed PLGS layer synchronously prolonged the release of insulin and exenatide after solidification. The circular dichroism spectra of exenatide were characterized by two minima around 208 and 222 nm, which is a typical fingerprint indicator of α-helix (Figure 4b). The circular dichroism spectrum of released exenatide agreed with that of native exenatide, indicating that the secondary structure of exenatide was well-preserved during the encapsulation and release process.

To induce type 2 diabetes, rats were placed on a 60 kcal% fat diet and injected intraperitoneally with a dose of 30 mg kg^{-1} streptozotocin (Figure 4c). Rats with type 2 diabetes were divided into five groups and subcutaneously injected with insulin&exenatide solution (insulin: 7.5 IU kg^{-1}, exenatide: 0.3 mg kg^{-1}), INS+EXE@PLGS (insulin: 50 IU kg^{-1}, exenatide: 2.08 mg kg^{-1}), INS@PLGS (50 IU kg^{-1}), EXE@PLGS (2.08 mg kg^{-1}), and N.S.

INS+EXE@PLGS increased the blood insulin and exenatide concentration for more than 8 days with a maximum plasma concentration of 33.4 mIU mL^{-1} for insulin and 67.2 ng mL^{-1} for exenatide (Figure 4d–f). For solution group, the plasma insulin and exenatide concentration peaked at 39.1 mIU mL^{-1} and

116.0 ng mL^{-1}, respectively, within 2 h after administration; the plasma concentration for both peptides declined rapidly. After encapsulation, the mean residence time of insulin and exenatide was remarkably prolonged from 0.3 to 4.8 days ($P < 0.001$) and from 0.09 to 4.3 days ($P < 0.001$), respectively (Figure 4g); the half-life of insulin and exenatide were 7.0 and 62.0 times ($P < 0.001$) higher than that of the corresponding peptide in solution group (Figure 4h). Thanks to its controlled release capability for peptides, INS+EXE@PLGS enhanced the bioavailability of insulin and exenatide for 1.6 and 2.7 times, respectively, when compared with the corresponding peptide in solution group (Figure 4i).

The blood glucose level of type 2 diabetic rats administrated with insulin&exenatide solution declined rapidly to approximately 177.3 mg dL^{-1} at 2 h after administration and increased back to the initially hyperglycemic state (421.5 mg dL^{-1}) at 8 h after administration (Figure 4j). INS+EXE@PLGS reduced the glycemia to 121.2 mg dL^{-1} at 2 h after administration and maintained the blood glucose level within the normal range for at least 8 days. The blood glucose level returned to hyperglycemic state (430.2 mg dL^{-1}) until 10 days after administration for INS+EXE@PLGS. As a result, the glucose area under curve for INS+EXE@PLGS (1.2 g dL^{-1}*d) was significantly ($P < 0.001$) lower than that of insulin&exenatide solution (3.5 g dL^{-1}*d) (Figure 4k). In contrast, with the administrated dose of insulin (50 IU kg^{-1}) and exenatide (2.08 mg kg^{-1}), single peptide encapsulated microcomposites, INS@PLGS and EXE@PLGS, did not show efficient glycemic control on type 2 diabetic rats (see Figure S14, Supporting Information).

As type 2 diabetes progresses, the risk of weight gaining increases, which further worsens hyperinsulinemia, hyperglycaemia, dyslipidemia, and insulin resistance.[50] As expected, the bodyweight of type 2 diabetic rats increased gradually during the whole therapy period (see Figure S15, Supporting Information). INS@PLGS accelerated this weight gaining, while the EXE@PLGS decreased the relative body weight to about 86.7% after 8 days. For INS+EXE@PLGS, the relative body weight decreased to 92.9% at 8 days after administration (Figure 4l). After the exhaustion of exenatide from INS+EXE@PLGS, the relative body weight increased gradually. In contrast, the relative bodyweight of type 2 diabetic rats injected with insulin&exenatide solution increased gradually. These bodyweight results demonstrated that the combination of exenatide with insulin could mitigate the weight gain associated with insulin. This phenomenon was in accidence with previous studies and could be ascribed to the delayed gastric emptying caused by exenatide.[24,49]

Collectively, INS+EXE@PLGS successfully optimized the pharmacokinetic features of insulin and exenatide synchronously and efficiently controlled the glycemic level in type 2 diabetic rats for 8 days. The combination of insulin and exenatide led to the mitigation of weight gain in type 2 diabetic rats. In conclusion, INS+EXE@PLGS might provide a new paradigm for the glycemic control of type 2 diabetes.

2.5. Co-Delivery of Insulin and Exenatide has Long-Term Therapeutic Efficacy in Type 2 Diabetic Rats

Since INS+EXE@PLGS could persist for 8 days, type 2 diabetic rats were subcutaneously injected with INS+EXE@PLGS (insulin: 50 IU kg^{-1}, exenatide: 2.08 mg kg^{-1}) once per week to evaluate its long-term therapeutic efficacy (**Figure 5**a). INS@PLGS (50 IU kg^{-1}), EXE@PLGS (2.08 mg kg^{-1}) and N.S. served as controls.

Once-weekly administration maintained the plasma insulin and exenatide level within the range of 12.6–35.6 mIU mL^{-1} and 13.7–49.3 ng mL^{-1}, respectively (Figure 5b). As a result, INS+EXE@PLGS revealed a tight glycemic control within 28 days (Figure 5c). By contrast, the rats were still hyperglycemic after the administration of INS@PLGS, EXE@PLGS, and N.S. The glucose area under the curve of INS+EXE@PLGS group was 3.6 g dL^{-1}*d, which was significantly ($P < 0.001$) lower than that of N.S. group (16.0 g dL^{-1}*d, see Figure S16, Supporting Information). After 4 weeks of treatment, the relative body weight of rats in N.S.-treated controls climbed to approximately 111.8% (Figure 5d); INS@PLGS increased this value to about 119.1%. Contrastively, rats in INS+EXE@PLGS group only gained 4.4% extra weight after 4 weeks, when compared with the initial state. EXE@PLGS even decreased the relative body weight to 93.2%. The change of relative body weight was consistent with that of a single dose.

HbA1c is less sensitive to daily glycemic fluctuations and is an integrated indicator over an extended period.[28] Therefore, we monitored the percentage of HbA1c during the whole therapeutic period. Prior to treatment, HbA1c levels for INS+EXE@PLGS, INS@PLGS, EXE@PLGS, and N.S. groups were all in the range of 5.7–5.9% (Figure 5e). After 4 weeks of treatment, HbA1c level in INS+EXE@PLGS group (4.3 ± 0.2%) was significantly lower than that of N.S.-treated control group (12.7 ± 0.7%). The 4 weeks treatment of INS+EXE@PLGS successfully controlled the blood glucose level within the normal range, efficiently slowed their body weight gain, and significantly reduced the HbA1c level in type 2 diabetic rats.

3. Conclusion

In summary, we successfully developed a surface adsorption strategy to fabricate microcomposites encapsulated with single-, dual-, or triple-peptide therapeutics with ultrahigh loading degree and precise ratiometric control. In this strategy, we formulated the peptide molecules into nanoparticles, and decorated the nanoparticle surface with PLGS. The adsorbed PLGS layer blocked the phase transfer of peptide nanoparticles from oil to water. As a result, the fabricated microcomposites revealed a loading degree up to 78.9%, which is ultrahigh for peptide therapeutics. After surface adsorption, all three peptide nanoparticles uniformly exhibited the properties of adsorbed PLGS. The uniform surface property of peptide nanoparticles enabled the co-encapsulation of three peptides with a precise ratiometric control. The release of peptides was synchronously prolonged after the solidification of adsorbed PLGS layer. INS@PLGS and INS+EXE@PLGS extended half-life and mean residence time for encapsulated peptides and improved their bioavailability. As a result, a single injection of INS@PLGS achieved an 8-day glycemic control in type 1 diabetic rats; INS+EXE@PLGS efficiently controlled the glycemic level in type 2 diabetic rats for 8 days. Weekly administration of INS+EXE@PLGS successfully maintained a steady plasma
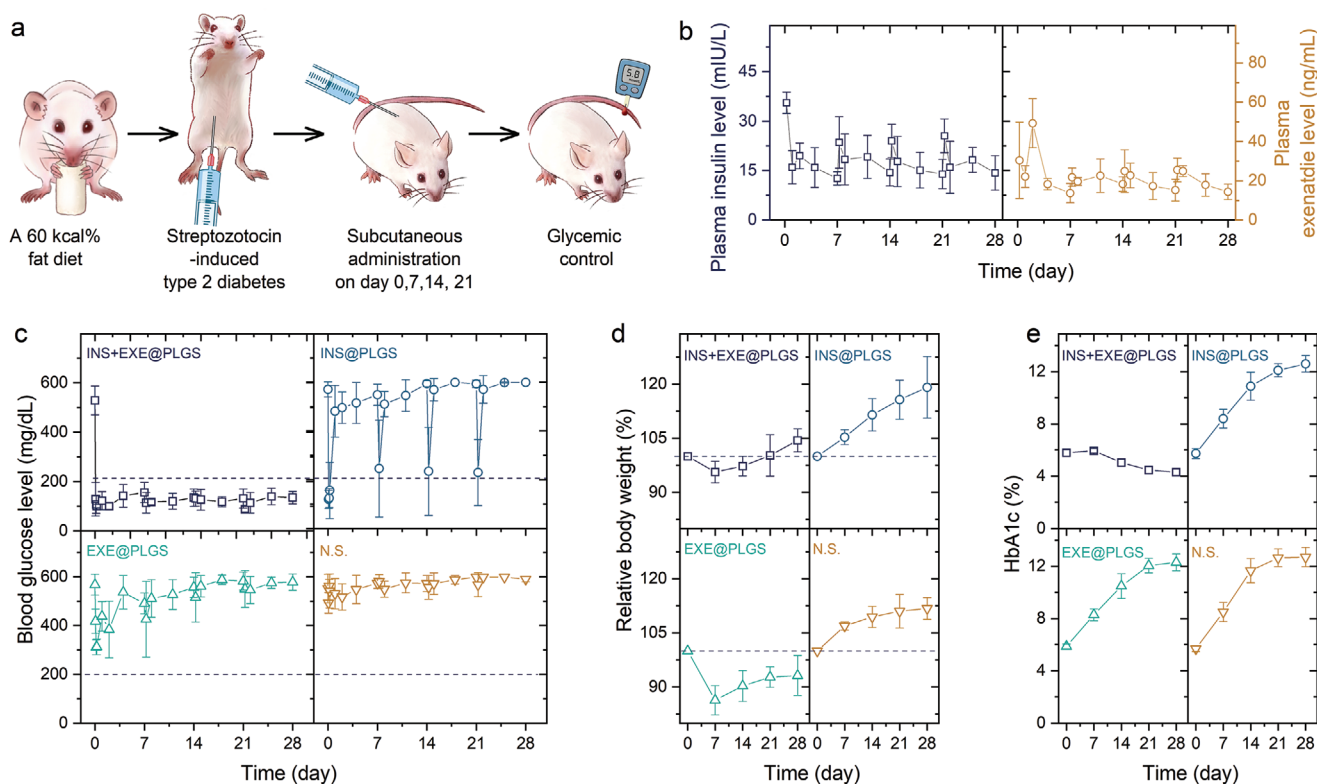
ADVANCED
SCIENCE NEWS
www.advancedsciencenews.com

NANO · MICRO
small
www.small-journal.com

Figure 5. Co-delivery of insulin and exenatide has long-term therapeutic efficacy in type 2 diabetic rats. a) Schematic diagram of long-term in vivo study in type 2 diabetic rats. b) Plasma insulin and exenatide level of type 2 diabetic rats administrated once per week with INS+EXE@PLGS ($n = 6$). c–e) Blood glucose levels (c), relative body weight (d), and HbA1c level (e) of type 2 diabetic rats subcutaneously administrated with INS+EXE@PLGS, INS@PLGS, EXE@PLGS, and N.S. once per week ($n = 6$).

drug concentration on type 2 diabetic rats, and thus, effectively reduced their weight gain and HbA1c level. Such improved pharmacokinetic and pharmacodynamic features for encapsulated peptides could vastly reduce the administration frequency and enhance the therapeutic outcomes and patient compliance.

4. Experimental Section

Preparation of Peptide Nanoparticles: All peptide nanoparticles were prepared through nanoprecipitation method. Insulin nanoparticles were fabricated by adding poor solvent, acetone (5 mL), into insulin aqueous solution (0.012 M HCl, 0.5 mL, 20 mg mL^{-1}) dropwise with moderate stirring. Exenatide nanoparticles were manufactured through modified methods, which replaced the poor solvent with acetonitrile. For bivalirudin, acetonitrile (3 mL) was added into bivalirudin aqueous solution (0.2 mL, 50 mg mL^{-1}) dropwise with moderate stirring. The size and size distribution of the peptide particles was measured employing a Zetasizer Ultra (Malvern Instruments Ltd., UK) at 25 °C with an angle of 173°.

Quartz Crystal Microbalance: The adsorption of polymers (PLGA and PLGS) onto insulin and exenatide particles was evaluated by a QSense Analyzer (Biolin Scientific AB, Gothenburg, Sweden). To form peptide films, insulin or exenatide particles suspension in dimethyl carbonate were added onto a sensor (QSX303 SiO$_2$, Biolin Scientific AB, Gothenburg, Sweden) and step spin-coated (800 rpm, 15 s; 4000 rpm, 30 s) for three times. The sensor coated with insulin or exenatide particles was placed in the flow cell and stabilized by introducing dimethyl carbonate into the flow module. Afterwards, polymers dimethyl carbonate solutions (10 mg mL^{-1}) flowed over the sensor surface for approximately 20 min. Finally, the dimethyl carbonate was introduced

into the flow module again to remove the unbonded polymers. All experiments were conducted at 25 °C and with a flow mode of 0.5 mL min^{-1} for three times. During the experiment, the changes of frequency and dissipation were recorded and all results were analyzed through a QSense Dfind (Biolin Scientific AB, Gothenburg, Sweden).

Phase Transfer of Peptide across Oil and Water Interface: The phase transfer of insulin and exenatide particles was studied employing a Cary 3500 UV–vis Spectrophotometer (Agilent Technologies Inc., U.S.). In the cuvette, water (1.5 mL) was stacked on the top of dimethyl carbonate (0.5 mL) containing insulin or exenatide particles without or with polymers (PLGA and PLGS). The water and oil phases were stirred at 400 rpm simultaneously. The amount of insulin or exenatide transferred into water phase was measured by the UV–vis Spectrophotometer (Agilent Technologies Inc., U.S.).

Engineering of Microcomposites: Dimethyl carbonate (15 mL for insulin, 15 mL for exenatide, and 40 mL for bivalirudin) was added into the prepared peptide nanoparticles, and the sample was centrifuged at 3000 rpm for 5 min. The precipitated peptide nanoparticles were redispersed in PLGS dimethyl carbonate solution by tip sonication with an amplitude of 20% for 30 s. The peptide-encapsulated microcomposites were fabricated employing a flow-focusing device. Briefly, polyvinyl alcohol solution (1%, w/v) and dimethyl carbonate-containing peptide nanoparticles and PLGS served as continuous phase and dispersed phase, respectively. The continuous phase pumped into the space between inner and outer capillaries, while the dispersed phase flowed into outer capillary in the opposite direction. Oil-in-water droplets were formed in the inner capillary and collected in polyvinyl alcohol aqueous solution (1%, w/v). After depletion of dimethyl carbonate, the emulsions solidified into microcomposites, which were washed with Milli-Q water for three times to remove polyvinyl alcohol thoroughly. The total concentration of peptides and polymer in the oil

phase was 20 mg mL^{-1}. Besides, when preparing bare microparticles for the cytocompatibility and in vivo experiments, oil phase was replaced with PLGS dimethyl carbonate solution (20 mg mL^{-1}).

Characterization of Peptide-Encapsulated Microcomposites: To measure the encapsulation efficiency and loading degree of insulin, exenatide, and bivalirudin in the microcomposites, the microcomposites were freeze-dried and dissolved in dimethyl sulfoxide to release all peptide molecules. The amount of peptide molecules encapsulated in the microcomposites was measured by a 1260 Infinity II high-performance liquid chromatography (Agilent Technologies, USA). Besides, the morphology of the obtained microcomposites was observed through a Zeiss Axio Observer 7 microscope (Carl Zeiss AG, Germany) and their size distribution was analyzed using ImageJ software.

Drug Release Test: To study the in vitro peptide release from INS@PLGS and INS+EXE@PLGS, microcomposites were suspended in 1 mL phosphate buffer (pH 7.4) under the sink condition. All samples were incubated at 37 °C with shaking (150 rpm). At prescribed time intervals, the samples were centrifuged (3000 rpm, 5 min) and the supernatant was removed. Afterwards, 1 mL fresh phosphate buffer (pH 7.4) was added. The insulin or exenatide concentrations in the supernatant were measured through a 1260 Infinity II high-performance liquid chromatography (Agilent Technologies, USA). The stability of the released insulin and exenatide was evaluated using a Jasco J-810 circular dichroism spectropolarimeter (JASCO International Co., Ltd., Japan). The insulin and exenatide standard solution were prepared in phosphate buffer (pH 7.4) and water, respectively. And both the concentration of insulin and exenatide were 0.1 mg mL^{-1}. All experiments were conducted at 25 °C and the length of the cell was 0.1 cm. All samples were scanned from 190 to 260 nm with a resolution of 1 nm and scanning speed of 50 nm min^{-1}.

Diabetes Model: The treatment efficacy of the INS@PLGS and INS+EXE@PLGS was evaluated in vivo employing streptozotocin-induced type 1 and 2 diabetic SD rats (male, $n = 6$), respectively. Rats were cared for under the supervision of China Pharmaceutical University and in compliance with protocols approved by China Pharmaceutical University Institutional Animal Care and Use Committee (202 103 003). To induce type 1 diabetes, rats were fasted overnight and intraperitoneally injected with streptozotocin (50 mg kg^{-1}) in citrate buffer (pH 4.5). For the type 2 diabetes model, rats were placed on a 60 kcal% fat diet for 4 weeks and intraperitoneally injected with streptozotocin (30 mg kg^{-1}) in citrate buffer (pH 4.5). The blood glucose levels of rats were measured through a Contour Plus (Bayer Consumer Care AG, Germany) and rats with blood glucose levels higher than 400 mg dL^{-1} were used for the in vivo experiments.

Pharmacokinetic and Pharmacodynamic Studies for INS@PLGS: To evaluate the pharmacodynamics of INS@PLGS, type 1 diabetic rats were divided into four groups and subcutaneously injected with free insulin solution (10 IU kg^{-1}), INS@PLGS microcomposites (100 IU kg^{-1}) dispersed in carboxymethylcellulose solution (2%, w/v; 1 mL), bare PLGS microparticles, and N.S., respectively. Furthermore, normal rats were served as control. At prescribed time intervals, their blood glucose level and body weight were monitored. All blood glucose levels were measured in the morning (9:00–11:00 am) except those within 8 h after administration. To evaluate the pharmacokinetic of INS@PLGS, venous blood of rats injected with insulin solution and INS@PLGS microcomposites was collected in BD Vacutainer (Becton Dickinson and Company, USA). Afterwards, the blood samples were centrifuged (1000×g, 10 min) and the upper plasma was taken out. The plasma was stored at −80 °C until assayed. Human/Canine/Porcin Insulin ELISA kit (MultiSciences, China) was employed to measure the plasma insulin level under the manufacturer's instruction.

Histochemical Evaluation of Tissue Adjacent to Injection Site: Histological analysis was conducted to evaluate the tissue biocompatibility of INS@PLGS microcomposites. At 0, 5, 10, and 16 days after administration, the subcutaneous tissue adjacent to the administration site was excised from the rats. The removed tissues were fixed in 4% paraformaldehyde solution and embedded in paraffin wax, which were sectioned into slices (3–5 um). The slices stained with DAPI and anti-CD68 were imaged by a microscope (Axio Observer 7, Carl Zeiss AG, Germany). Finally, the fraction of CD68-positive cells were analyzed by VTEA plugin of ImageJ.[48]

Pharmacokinetic and Pharmacodynamic Studies of INS+EXE@PLGS: Type 2 diabetic rats were divided into five groups and they were subcutaneously administrated with free insulin&exenatide solution (insulin: 7.5 IU kg^{-1}, exenatide: 0.3 mg kg^{-1}), INS+EXE@PLGS (insulin: 50 IU kg^{-1}, exenatide: 2.08 mg kg^{-1}), INS@PLGS (50 IUkg^{-1}), EXE@PLGS (2.08 mg kg^{-1}), and N.S., respectively. Rats without hyperglycemia served as control. After the administration, their plasma insulin concentration, plasma exenatide concentration, blood glucose levels, and body weight were monitored over time. The plasma insulin concentration and plasma exenatide concentration were measured using Human/Canine/Porcin Insulin ELISA kit (MultiSciences, China), and Exendin-4 EIA kit (Phoenix Pharmaceutics, Inc., USA), respectively.

Long-Term Therapeutic Efficacy of INS+EXE@PLGS: Type 2 diabetic rats were divided into four groups and administrated with INS+EXE@PLGS (insulin: 50 IU kg^{-1}, exenatide: 2.08 mg kg^{-1}), INS@PLGS (50 IU kg^{-1}), EXE@PLGS (2.08 mg kg^{-1}), and N.S., respectively, weekly for 4 weeks. Their plasma insulin concentration, plasma exenatide concentration, plasma glucose level, body weight, and HbA1c level were measured and recorded periodically. HbA1c was measured using a A1CNow Self Check (Sinocare Inc., China).

Statistical Analysis: All data were replicated at least three times. Statistical analysis was performed using one-way analysis of variance (ANOVA) followed by a Bonferroni's post hoc test for multiple comparisons of OriginPro 2020 software (Origin lab corporation, USA). Pharmacokinetic parameters, including maximum plasma concentration, half-life, mean residence time, and area under curve, were calculated from the plasma concentration-time curve by PKSolver.[51] The time for the pharmacokinetic parameter calculation of solution and microcomposites groups were 2 and 16 days, respectively. The relative bioavailability was calculated by dividing the mean area under curve value of microcomposite group by that of the solution group.

Supporting Information

Supporting Information is available from the Wiley Online Library or from the author.

Acknowledgements

Conflict of Interest

The authors declare no conflict of interest.

Author Contributions

P.Z., C.D., and T.H. contributed equally to this work. D.L., H.A.S., and P.Z. conceived and designed the experiments. P.Z., C.D., T.H., S.H., Y.B., C.L., Y.G., Z.L., and B.W. performed the experiments. D.L., J.T.H., J.F., and H.A.S. guided the experiments. P.Z. analyzed and interpreted the data. P.Z. and D.L. wrote the paper. All authors discussed the results and commented on the manuscript.

[1] D. Elias, I. R. Cohen, *Lancet* **1994**, *343*, 704.

[2] H. Offner, G A. Hashim, A. A. Vandenbark, *Science* **1991**, *251*, 430.

[3] L. Agemy, D. Friedmann-Morvinski, V. R. Kotamraju, L. Roth, K. N. Sugahara, O. M. Girard, R. F. Mattrey, I. M. Verma, E. Ruoslahti, *Proc. Natl. Acad. Sci. U. S. A.* **2011**, *108*, 17450.

[4] H. Kaneto, Y. Nakatani, T. Miyatsuka, D. Kawamori, T.-A. Matsuoka, M. Matsuhisa, Y. Kajimoto, H. Ichijo, Y. Yamasaki, M. Hori, *Nat. Med.* **2004**, *10*, 1128.

[5] S. Fernandez-Lopez, H. -S. Kim, E C. Choi, M. Delgado, J R. Granja, A. Khasanov, K. Kraehenbuehl, G. Long, D A. Weinberger, K M. Wilcoxen, M. R Ghadiri, *Nature* **2001**, *412*, 452.

[6] U. Silphaduang, E. J. Noga, *Nature* **2001**, *414*, 268.

[7] D. J. Drucker, *Nat. Rev. Drug Discovery* **2019**, *19*, 277.

[8] R. Menacho-Melgar, J. S. Decker, J. N. Hennigan, M. D. Lynch, *J. Controlled Release* **2019**, *295*, 1.

[9] E. L. Hedberg, A. Tang, R. S. Crowther, D. H. Carney, A. G. Mikos, *J. Controlled Release* **2002**, *84*, 137.

[10] L. E. Bromberg, E. S. Ron, *Adv. Drug Delivery Rev.* **1998**, *31*, 197.

[11] J. J. Meier, *Nat. Rev. Endocrinol.* **2012**, *8*, 728.

[12] J. Liu, Y. Xiao, C. Allen, *J. Pharm. Sci.* **2004**, *93*, 132.

[13] K. Letchford, R. Liggins, H. Burt, *J. Pharm. Sci.* **2008**, *97*, 1179.

[14] Yu Zhang, T. Ren, J. Gou, L. Zhang, X. Tao, B. Tian, P. Tian, D. Yu, J. Song, X. Liu, Y. Chao, W. Xiao, X. Tang, *J. Controlled Release* **2017**, *261*, 352.

[15] X. Ke, V. W. L. Ng, R. J. Ono, J. M. W. Chan, S. Krishnamurthy, Y. Wang, J. L. Hedrick, Y. Y. Yang, *J. Controlled Release* **2014**, *193*, 9.

[16] E. M. Enlow, J. C Luft, M E. Napier, J. M. Desimone, *Nano Lett.* **2011**, *11*, 808.

[17] J. S. Lee, P. Han, R. Chaudhury, S. Khan, S. Bickerton, M D. Mchugh, H. B. Park, A. L. Siefert, G. Rea, J. M. Carballido, D. A. Horwitz, J. Criscione, K. Perica, R. Samstein, R. Ragheb, D. Kim, T. M. Fahmy, *Nat. Biomed. Eng.* **2021**, *5*, 983.

[18] D. Lane, *Nat. Biotechnol.* **2006**, *24*, 163.

[19] M. J. Vicent, F. Greco, R I. Nicholson, A. Paul, P. C. Griffiths, R. Duncan, *Angew. Chem.* **2005**, *117*, 4129.

[20] J. Conde, N. Oliva, Yi Zhang, N. Artzi, *Nat. Mater.* **2016**, *15*, 1128.

[21] R. K. Jain, *Nat. Med.* **2001**, *7*, 987.

[22] P. D. Home, S. J. Pocock, H. Beck-Nielsen, P. S. Curtis, R. Gomis, M. Hanefeld, N. P. Jones, M. Komajda, J. J. V. McMurray, *Lancet* **2009**, *373*, 2125.

[23] A. D. Association, *Diabetes Care* **2018**, *8*, S73.

[24] W. Nuffer, A. Guesnier, J. M. Trujillo, *Ther. Adv. Endocrinol. Metab.* **2018**, *9*, 69.

[25] J. G. M. Klijn, *J. Natl. Cancer Inst.* **2000**, *92*, 903.

[26] F. Kratz, A. Warnecke, *J. Controlled Release* **2012**, *164*, 221.

[27] H. Meng, M. Liong, T. Xia, Z. Li, Z. Ji, J. I. Zink, A E. Nel, *ACS Nano* **2010**, *4*, 4539.

[28] K. M. Luginbuhl, J. L. Schaal, B. Umstead, E. M. Mastria, X. Li, S. Banskota, S. Arnold, M. Feinglos, D. D'alessio, A. Chilkoti, *Nat. Biomed. Eng.* **2017**, *1*, 0078.

[29] Y. Qi, A. Simakova, N. J. Ganson, X. Li, K. M. Luginbuhl, I. Ozer, W. Liu, M. S. Hershfield, K. Matyjaszewski, A. Chilkoti, *Nat. Biomed. Eng.* **2016**, *1*, 0002.

[30] J. Yu, J. Wang, Y. Zhang, G. Chen, W. Mao, Y. Ye, A R. Kahkoska, J. B. Buse, R. Langer, Z. Gu, *Nat. Biomed. Eng.* **2020**, *4*, 499.

[31] P. Mukhopadhyay, R. Mishra, D. Rana, P. P. Kundu, *Prog. Polym. Sci.* **2012**, *37*, 1457.

[32] M. E. Leunissen, A. Van Blaaderen, A. D. Hollingsworth, M. T. Sullivan, P. M. Chaikin, *Proc. Natl. Acad. Sci. U. S. A.* **2007**, *104*, 2585.

[33] A. Yethiraj, A. Van Blaaderen, *Nature* **2003**, *421*, 513.

[34] M. E. Leunissen, C. G. Christova, A. -P. Hynninen, C. P Royall, A. I. Campbell, A. Imhof, M. Dijkstra, R. Van Roij, A. Van Blaaderen, *Nature* **2005**, *437*, 235.

[35] E. Gurdak, C. C. Dupont-Gillain, J. Booth, C. J. Roberts, P. G. Rouxhet, *Langmuir* **2005**, *21*, 10684.

[36] L. Mivehi, R. Bordes, K. Holmberg, *Langmuir* **2011**, *27*, 7549.

[37] O. Wintersteiner, H. A. Abramson, *J. Biol. Chem.* **1933**, *99*, 741.

[38] Y. Shi, X. Sun, L. Zhang, K. Sun, K. Li, Y. Li, Q. Zhang, *Sci. Rep.* **2018**, *8*, 726.

[39] K. R Ratinac, O. C Standard, P. J Bryant, *J. Colloid Interface Sci.* **2004**, *273*, 442.

[40] C. Lourenco, *Int. J. Pharm.* **1996**, *138*, 1.

[41] M. C. Petersen, G. I. Shulman, *Physiol. Rev.* **2018**, *98*, 2133.

[42] E.-S. Khafagy, M. Morishita, Y. Onuki, K. Takayama, *Adv. Drug Delivery Rev.* **2007**, *59*, 1521.

[43] R. Mo, T. Jiang, J. Di, W. Tai, Z. Gu, *Chem. Soc. Rev.* **2014**, *43*, 3595.

[44] M. Brownlee, A. Cerami, *Science* **1979**, *206*, 1190.

[45] A. Matsumoto, T. Ishii, J. Nishida, H. Matsumoto, K. Kataoka, Y. Miyahara, *Angew. Chem., Int. Ed.* **2012**, *51*, 2124.

[46] H. Guo, H. Li, J. Gao, G. Zhao, L. Ling, B. Wang, Q. Guo, Y. Gu, C. Li, *Polym. Chem.* **2016**, *7*, 3189.

[47] Y. Yao, L. Zhao, J. Yang, J. Yang, *Biomacromolecules* **2012**, *13*, 1837.

[48] S. Winfree, S. Khan, R. Micanovic, M. T. Eadon, K. J. Kelly, T. A. Sutton, C. L. Phillips, K. W. Dunn, T. M. El-Achkar, *J. Am. Soc. Nephrol.* **2017**, *28*, 2108.

[49] R. O. Moreira, R. Cobas, R. C. L. A. Coelho, *Diabetol. Metab. Syndr.* **2018**, *10*, 26.

[50] R. Balena, I. E. Hensley, S. Miller, A. H. Barnett, *Diabetes, Obes. Metab.* **2013**, *15*, 485.

[51] Y. Zhang, M. Huo, J. Zhou, S. Xie, *Comput. Methods Programs Biomed.* **2010**, *99*, 306.